ELSEVIER

International Journal of Mass Spectrometry 202 (2000) 363–379

International Journal of Mass Spectrometry

# How does $Fe^+$ activate ethylsilane? A theoretical study in comparison with experiments

Susanne Bärsch, Detlef Schröder, Helmut Schwarz*

*Institut für Organische Chemie, Technische Universität Berlin, Straße des 17. Juni 135, D-10623 Berlin, Germany*

Received 17 May 2000; accepted 2 June 2000

**Abstract**

Based upon mass-spectrometric studies, the activation of ethylsilane by "naked" $Fe^+$ ions is computationally investigated using the B3LYP approach together with a basis set of valence double-$\zeta$ quality. In particular, the mechanistic details for the experimentally observed losses of neutral $H_2$, $CH_4$, and $SiH_4$, respectively, are investigated. According to the initial steps of bond activation, this requires the computation of four potential-energy surfaces, corresponding to insertion into the carbon–silicon (C–Si), carbon–hydrogen [C(1)–H and C(2)–H], and carbon–carbon (C–C) bonds; activation of the silicon–hydrogen (Si–H) bonds is ruled out on experimental grounds. Both quartet and sextet states of $Fe^+$ are taken into account. The agreement between theory and experiments is satisfactory because all products observed in the experiments are also calculated to proceed exothermically on the reaction surface, and the experimentally preferred exit channel is also predicted as the most favored reaction channel by the theoretical approach. (Int J Mass Spectrom 202 (2000) 363–379) © 2000 Elsevier Science B.V.

*Keywords:* B3LYP; Gas-phase chemistry; C–Si bond activation; Si–H bond activation; Ethylsilane

## 1. Introduction

Due to the inertness of C–H and C–C bonds as well as the similar strength of the different C–H and C–C bonds, even in small organic substrates, the exclusive activation of preselected positions in organic substrates is a task that is difficult to achieve. Nevertheless, extensive research has been carried out in this field during the last decades and quite some progress has been accomplished [1–4]. Studies in the solution phase involved selective activation of functionalized and unfunctionalized alkanes by means of tuning the reactivity of the activating reagent, i.e. the transition metal, by various ligands and/or choice of oxidation state [5–9]. In a very recent study [10], Hartwig and co-workers accomplished the highly regioselective conversion of alkanes in solution into organoboranes by use of a rhodium catalyst. Moreover, Davies et al. [11] even managed an asymmetric catalytic alkane activation by rhodium complexes. In contrast, gas-phase studies concentrated on the activation of small alkanes and functionalized substrates by "bare" transition metal ions or small transition-metal complexes such as metal oxides and sulfides in order to obtain information about the elementary steps of the reaction [12–14]. Especially during the last decades, since

* Corresponding author. E-mail: schw0531@www.chem.tu-berlin.de


*PII* S1387-3806(00)00262-1

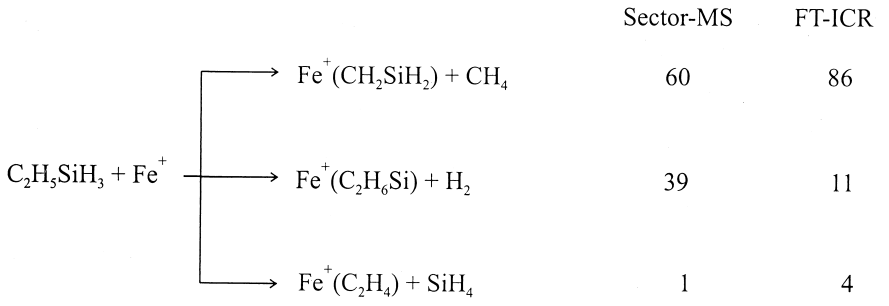


Fig. 1. Product distribution for $Fe^+$/ethylsilane in FTICR and sector-field MS experiments. The intensities are normalized to $\Sigma_{products} = 100\%$; ion intensities <1% are omitted.

computer technology has evolved so rapidly, *ab initio* calculations provide an important additional tool for the investigation of gas-phase chemistry [15–19].

Our group has contributed to the field of selective bond activation by the investigation of various substrates in the gas phase [12,20–23]. Recently, we published a study of the activation of *n*-propyltrimethylsilane by "bare" $Fe^+$ and $Co^+$ ions, and we found dramatic differences in the product selectivity of the two transition metals [24]. Because iron and cobalt are generally considered not to be so different chemically, this is a surprising result that was deemed worthy of further investigation. However, labeling experiments could not answer all the remaining mechanistic questions, and therefore, we searched for a system that shows similar reactivity differences for $Fe^+$ and $Co^+$ but is small enough to allow a detailed theoretical investigation. We chose ethylsilane (**1**) as a substrate for this investigation and the first part of our results, i.e. the activation of ethylsilane by "bare" cobalt cations has been published recently [25]. In this article we present a discussion of the $Fe^+$/ethylsilane PES.

## 2. Experiments

Prior to the theoretical treatment, the experimental results for the reaction of $Fe^+$ with $C_2H_5SiH_3$ are presented to define the scope of the theoretical investigation. The data of the two mass spectrometric techniques are displayed in Fig. 1.

Both Fourier transform ion cyclotron resonance (FTICR) and sector mass spectrometry show a strong preference for loss of neutral $CH_4$ concomitant with formation of $Fe(CH_2SiH_2)^+$, which is in marked contrast to the previously investigated $Co^+$/ethylsilane system. Eliminations of $H_2$ and $SiH_4$ are clearly much less pronounced. Note in that respect, that dihydrogen may be lost from different positions within the molecule; therefore, the formation of the isomeric products species $Fe(C_2H_3SiH_3)^+$ or $Fe(C_2H_5SiH)^+$ requires particular consideration.

Some additional insight into the mechanistic scenario is gained from a labeling experiment using $Fe^+/C_2H_5SiD_3$. In the sector MS, the deuterated products $CH_3D$ and $SiD_3H$ are observed exclusively, consistent with C–C and Si–D bond activation for methane formation and Si–C and C–H bond insertions for the production of silane. With regard to elimination of molecular hydrogen, no losses of HD or $D_2$ are observed in the $Fe^+/C_2H_5SiD_3$ system, even upon collisional activation. Thus, the structure of the ionic product appears to retain an intact silyl group, i.e. to $Fe(C_2H_3SiH_3)^+$ rather than the silylidene structure $Fe(C_2H_5SiH)^+$; interestingly, the latter was experimentally found to be formed from $Co^+$/ethylsilane [25].

## 3. Theoretical methods

Calculations are performed utilizing the program package GAUSSIAN 94 [26]. Because the system under investigation is of considerable size and requires large resources concerning computer time and memory requirements, the CRAY-YMP supercomputer at the

Konrad-Zuse-Zentrum Berlin is used. We employ density functional theory (DFT) at the B3LYP level of theory [27–29] for the following two reasons: (1) the B3LYP approach has been used widely for the description of transition-metal mediated activation of organic substrates and has been shown to provide reasonably accurate energetics in transition metal involving reactions [30,31]. (2) Due to limitations in computing resources and the size of the investigated system, DFT is a reasonable compromise as compared to the computational efforts associated with non-DFT, highly correlated *ab initio* methods.

The Ahlrichs valence double-$\zeta$ (VDZ) basis set is used for Fe, H, C, and Si [32]. To achieve a better description of the valence space, the basis for Fe was slightly modified, such that the coefficients remain the same, but the contractions for the five d functions were changed (instead of using 5d → (2d)/[32] from Ahlrichs and co-workers [32] we used 5d → (3d)/[311]). The complete basis therefore consists of the following basis functions and contractions: H (10s7p)/[4s3p], C (7s4p)/[3s2p], Si (10s7p)/[4s3p], and $Fe^+$ (14s8p5d)/[5s2p3d].

All structures discussed in the text correspond to stationary points obtained by full geometry optimizations with both the gradients as well as the displacements from analytical second derivatives below the standard convergence criteria [33]. Frequency analysis is used to characterize the stationary points. Transition structures (TS) are additionally verified by IRC (intrinsic reaction coordinate) [34,35] calculations, connecting the TS to the corresponding minima. To allow a more direct comparison with experimental results, all energies are corrected for the zero-point vibrational energy (ZPVE) contributions.

## 4. Theoretical results

Four different routes for the activation of ethylsilane by $Fe^+$ are calculated according to the conceivable primary insertion sites for the transition-metal ion, e.g. C–Si, C(2)–H, C(1)–H, and C–C bond activation (see Fig. 2). Based upon the results of the labeling experiments, primary Si–H bond insertion is not included. On each PES, the corresponding quartet and sextet states are considered. The following section is organized so that first the entrance channel and the encounter complexes are described. This is followed by a characterization of the remaining species along the four individual reaction pathways. The energetic and geometrical features of minima and transition structures for both quartet and sextet states are discussed in the order of their appearance in Fig. 2, and the respective minima are displayed in Scheme 1; transition structures connecting these minima are shown in Scheme 2. For the sake of clarity, Scheme 1 displays only the most stable conformers found for each minimum.

Before starting with the evaluation of structures and geometries, two general remarks are indicated. (1) For the construction of the PES only the most stable conformers are considered because the barriers for interconversion of the different conformers are assumed to be much lower than the barriers for cleavage and/or formation of covalent bonds. (2) Due to the known deficiency of the B3LYP approach for treating atoms accurately, the entrance channel ($Fe^+ + C_2H_5SiH_3$) is expected to be associated with a somewhat larger error than the remaining parts of the PES (see below). Therefore, the encounter complex **2** is used as the reference point for the relative energy scale of the PES. The overall error of the calculations is estimated to be $\pm 6$ kcal $mol^{-1}$, based on the average deviations of calculated bond dissociation energies and heats of formation of model processes [36,37] with known literature thermochemistry as well as comparison with earlier B3LYP calculations on "bare" transition-metal/alkane systems [19,25,31,38–40].

### 4.1. Reactants

The description of the $Fe^+/C_2H_3SiH_3$ entrance channel already illustrates one of the major problems of the B3LYP approach. The notorious shortcomings of B3LYP are its tendency to overestimate bond-dissociation energies [31,41] and the occurrence of large errors in the calculation of atoms [42,43]. The latter stems from the fact that the B3LYP method poorly describes the low-spin/high-spin separation in

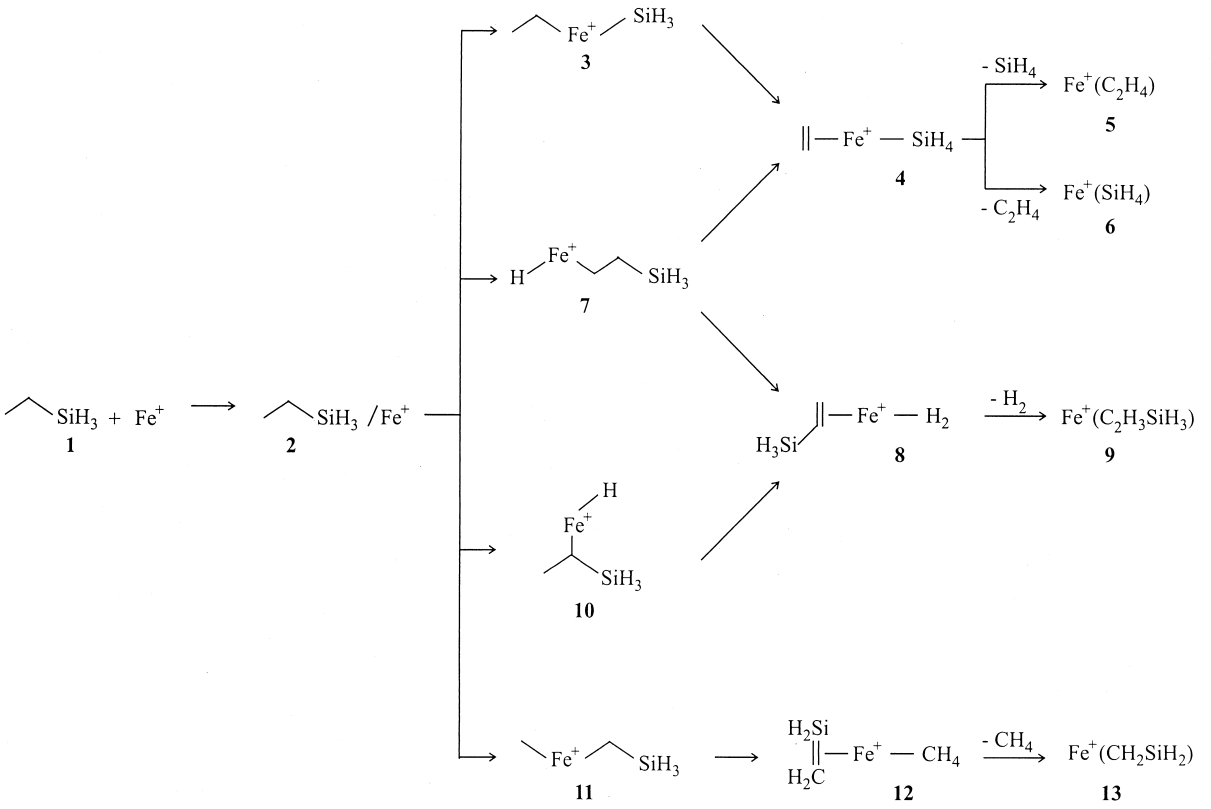


Fig. 2. Calculated reaction pathways of the $Fe^+$/ethylsilane system. Note that only the expected minima along the reaction coordinate are displayed whereas the transition structures are discussed in the text.

transition-metal atoms. This behavior is attributed to a bias of $3d^n$ over $3d^{n-1}4s^1$ configurations, leading to an artificial preference for the low spin $3d^n$ species [42–47]. Thus, the B3LYP/6-311+G* level of theory predicts $Fe^+$ ($^4F$) to be 4.1 kcal $mol^{-1}$ more stable than $Fe^+$ ($^6D$), whereas according to spectroscopic data, the $Fe^+$ cation has a $^6D$ ground state with a $3d^64s^1$ configuration that is 5.8 kcal $mol^{-1}$ lower in energy compared to $Fe^+$ ($^4F$) [48]. Therefore, the erroneous ground state assignment of atomic ions leads to increased uncertainties in the computed bond-dissociation energies of $M(L)^+$ complexes (L = ligand). The optimized structure of ethylsilane (**1**) exhibits $C_S$ symmetry and a $^1A'$ ground state. Note that we keep the numbering of the two carbon atoms in ethylsilane as C(1) and C(2) throughout the whole description of the $Fe^+$/ethylsilane system. Furthermore, the lengths of the Si–C, C–H, C–C, and Si–H bonds in neutral ethylsilane are used as internal references for typical single bonds between these elements.

### *4.2. Encounter complexes*

The lowest-lying quartet encounter complex $^4$**2** is assigned to $E_{rel}$ = 0 kcal $mol^{-1}$ on the energy scale. This $\eta^4$ complex is of $C_1$ symmetry and characterized by the interaction of the iron cation with the silicon atom, C(2), and two hydrogen atoms. Three other conformers of **2** are located on the quartet surface at relative energies of 1.1, 4.8, and 7.5 kcal $mol^{-1}$, i.e. $^4$**2′**, $^4$**2″**, and $^4$**2‴** (all not shown). Whereas $^4$**2′** is also a $\eta^4$ complex with interactions between iron and C(1), Si, and two hydrogen atoms, the $\eta^3$ complex $^4$**2″** shows only strong interaction between the iron cation and silicon as well as two hydrogen atoms on silicon, respectively. These structures have a silicon-iron in-

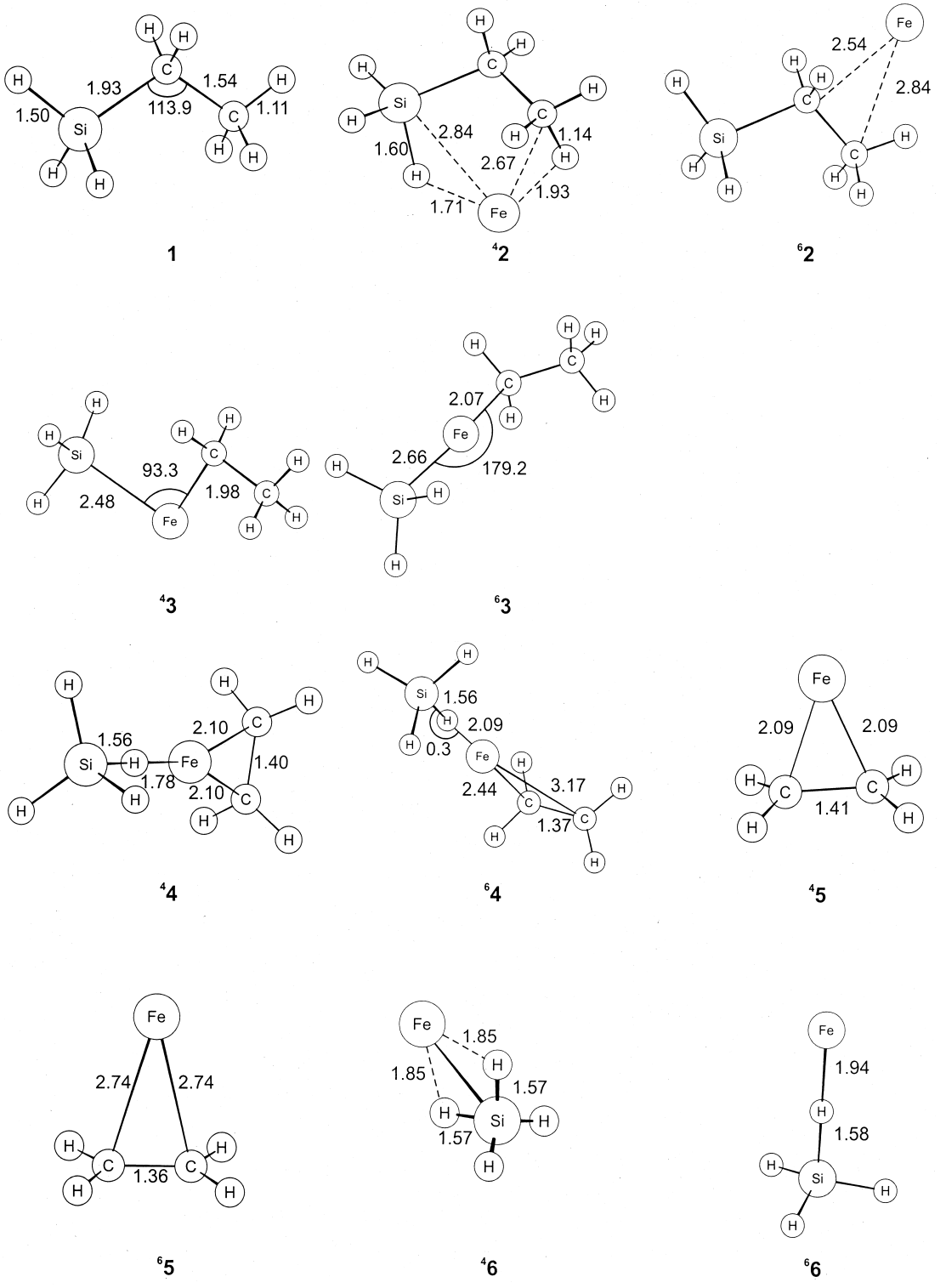
1.93
1.54
1.50
113.9
1.11
1
2.84
1.14
1.60
2.67
1.71
1.93
4 2
2.54
2.84
6 2
93.3
1.98
2.48
4 3
2.07
2.66
179.2
6 3
1.56
2.10
1.40
1.78
2.10
4 4
1.56
2.09
0.3
2.44
3.17
1.37
6 4
2.09
2.09
1.41
4 5
2.74
2.74
1.36
6 5
1.85
1.85
1.57
1.57
4 6
1.94
1.58
6 6

Scheme 1.

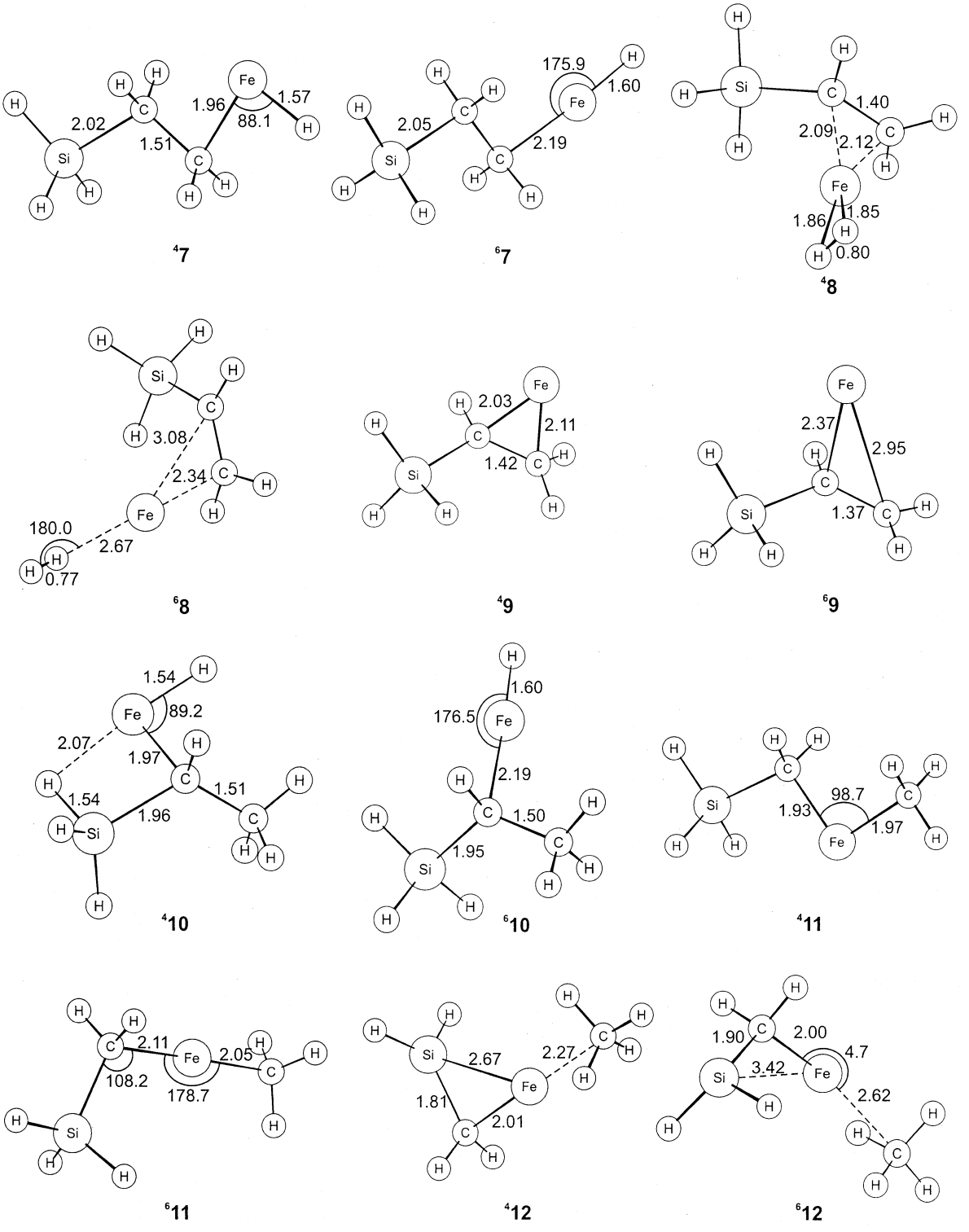


Scheme 1. (continued)

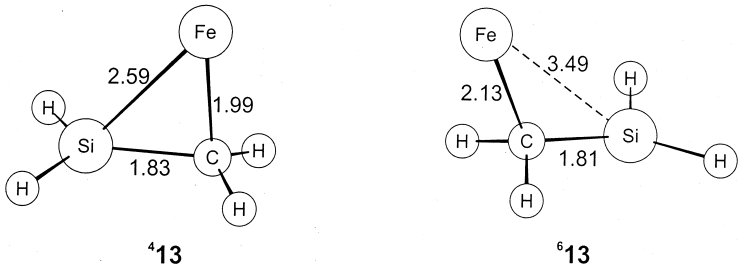


Scheme 1. (continued)

teraction in common, whereas in the least stable structure $^4$**2‴** the iron cation interacts only with C(1) and the two hydrogen atoms on C(1). The lower stability of $^4$**2‴** as compared to the other encounter complexes indicates a stronger interaction between the $Fe^+$ and silyl group as compared to the less pronounced $Fe^+$-methyl interaction. On the sextet surface, only one encounter complex $^6$**2‴** ($E_{rel}$ = 16.7 kcal mol$^{-1}$) is located, which corresponds structurally to $^4$**2‴**. Due to the high relative energy, further searches for encounter complexes along the sextet surface were not pursued.

### *4.3. C–Si insertion (Fig. 3)*

This pathway continues via TS**2**/**3** to the inserted structure **3**. The corresponding TS could not be located on either PES; however, previous experiences in our group with similar systems [25] as well as publications of the PESs of metal-mediated activations of simple alkanes [38–40] and functionalized substrates [30] show that the TSs from the encounter complexes to the primary insertion structures are generally lower in energy than the subsequent TSs associated with migration processes. A similar conclusion was drawn from experimental work [49–51]. Therefore, TS**2**/**3** is not likely to kinetically control the overall reactivity of the system.

Two C–Si inserted structures are localized on the quartet surface of which $^4$**3**, the *anti*-conformer with respect to the Fe–C bond, is the minimum at $E_{rel}$ = 5.7 kcal mol$^{-1}$. The second conformer $^4$**3′** ($E_{rel}$ = 6.2 kcal mol$^{-1}$, not shown) has a *gauche*-conformation and is therefore slightly energetically destabilized as compared to $^4$**3**. On the sextet surface, $^6$**3** ($E_{rel}$ = 21.7 kcal mol$^{-1}$) deviates from its quartet analog by an almost linear Si–Fe–C(1)-unit, a phenomenon that is observed on several occasions during this study and can be attributed to the different electronic structure of $^6Fe^+$ compared to $^4Fe^+$. Because all the 3d and 4s valence orbitals are occupied in $Fe^+$($^6$D), formation of covalent bonds or donation of electron density into an empty orbital as in a $\pi$ interaction is not possible, thus resulting in longer, electrostatic bonds formed by the sextet species as well as the observed linear arrangement of the fragments.

The reaction proceeds by $\beta$-H migration via TS**3**/**4** to complex **4**. On the quartet surface, $^4$TS**3**/**4** ($E_{rel}$ = 34.9 kcal mol$^{-1}$) shows an elongated C(2)–H bond along with intermediate formation of an Fe–H bond. The imaginary mode of i1040 cm$^{-1}$ corresponds mainly to the motion of the hydrogen atom from C(2) to Si with smaller contributions due to the planarization of the remaining hydrogen atoms on C(1) and C(2). The structure of $^6$TS**3**/**4** ($E_{rel}$ = 42.4) differs from $^4$TS**3**/**4** in that the Fe–Si bond is already very elongated ($r_{FeSi}$ = 3.55 Å) with the $SiH_3$ unit bent toward the $C_2$ unit. Thus, no intermediate Fe–H bond formation occurs in the sextet TS ($r_{FeH}$ = 2.65 Å). The imaginary frequency of i804 cm$^{-1}$ corresponds mainly to the motion of the hydrogen atom away from C(2) toward Si, accompanied by some contributions from the hydrogen atoms remaining at C(2).

Complex **4**, which is reached next, consists of the metal surrounded by two ligands, i.e. ethylene and silane. On the quartet surface, two conformers are located, i.e. $^4$**4** and $^4$**4′** ($E_{rel}$ = −14.1 and −11.4 kcal mol$^{-1}$). In the energetically favorable conformer $^4$**4**,

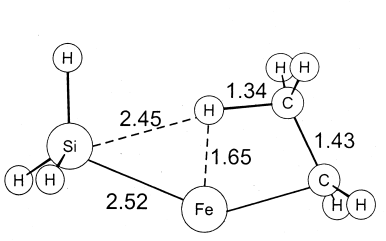


$^4$TS**3**/**4**

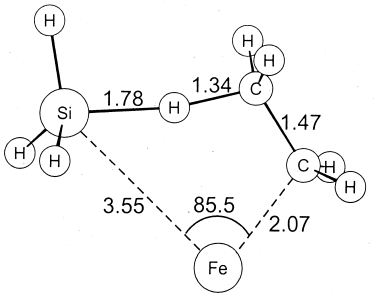


$^6$TS**3**/**4**

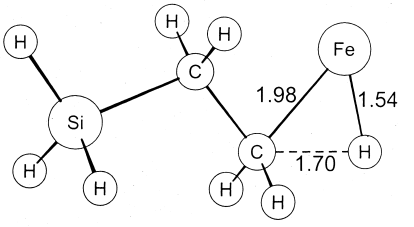


$^4$TS**2**/**7**

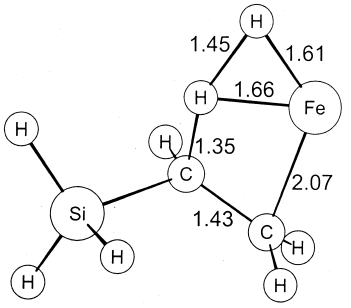


$^4$TS**7**/**8**

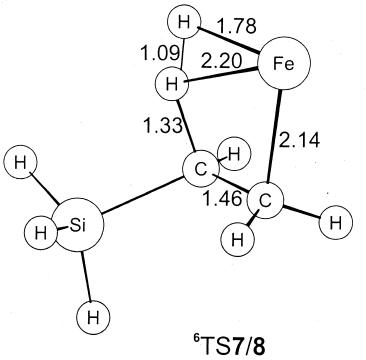


$^6$TS**7**/**8**

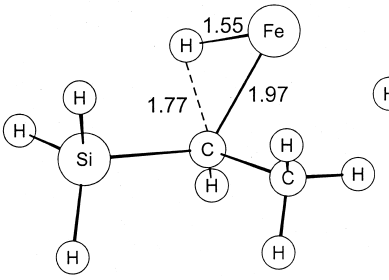


$^4$TS**2**/**10**

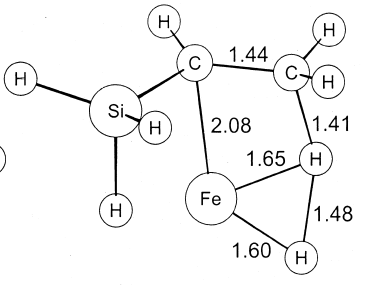


$^4$TS**8**/**10**

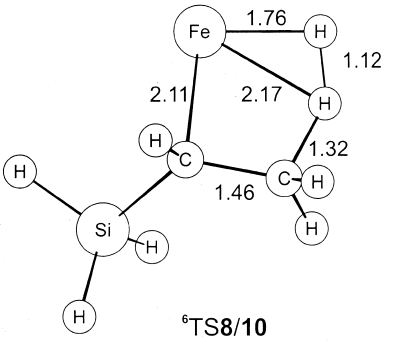


$^6$TS**8**/**10**

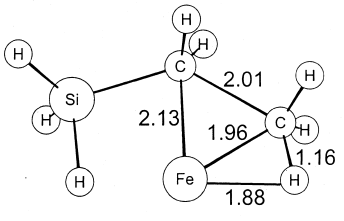


$^4$TS**2**/**11**

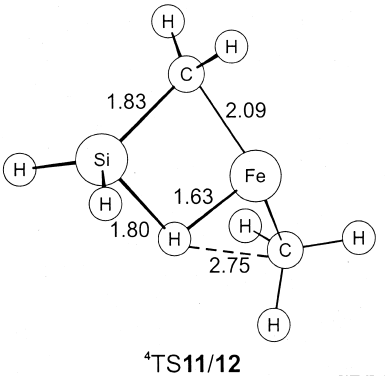


$^4$TS**11**/**12**

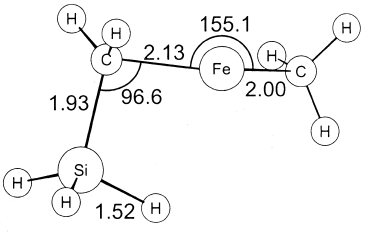


$^6$TS**11**/**12**

Scheme 2.

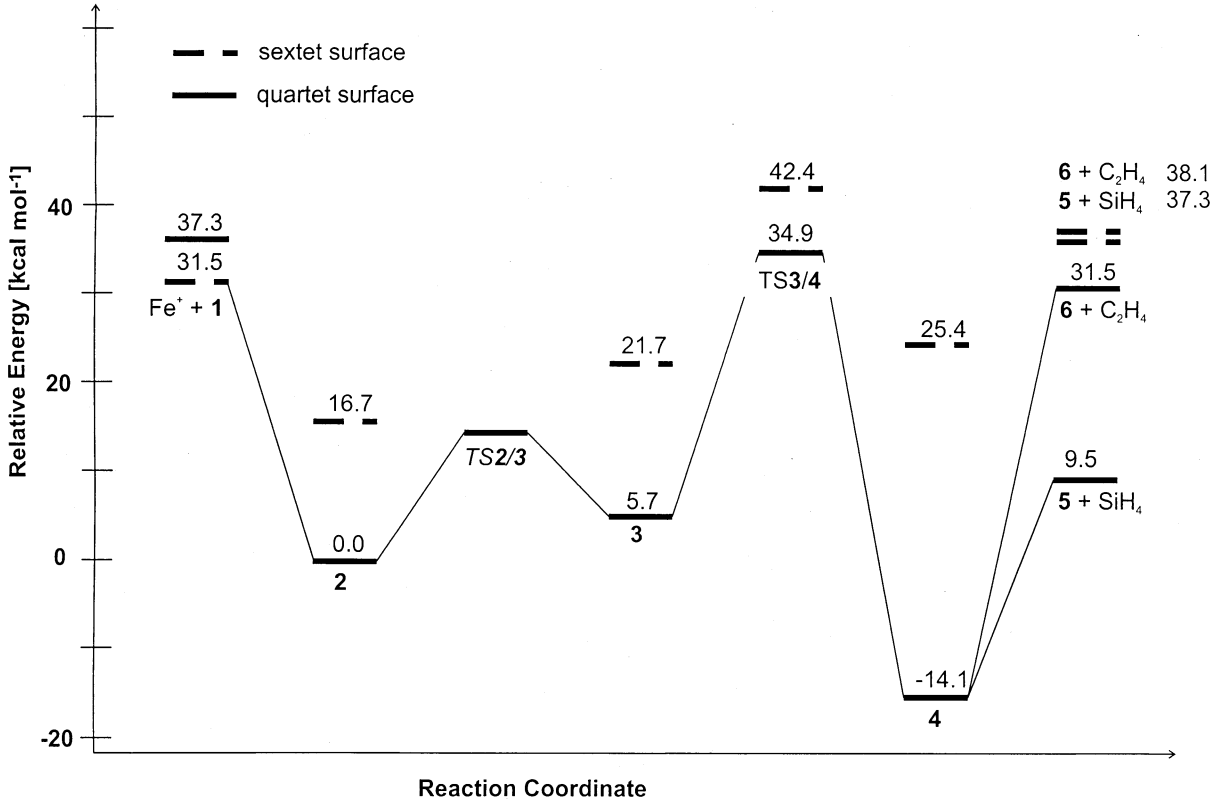


Fig. 3. B3LYP/Ahlrichs PES of the C–Si bond insertion pathway of $Fe^+ + C_2H_5SiH_3$ relative to the lowest-lying encounter complex $^4$**2**; ZPVE corrections are included, and the relative energetics are given in kcal $mol^{-1}$. The solid lines refer to the quartet structures whereas the dashed lines are used to denote the sextet structures.

the silane molecule is bound to $Fe^+$ through an electrostatic interaction of one hydrogen atom of the silane molecule with the iron cation; hence, the hydrogen atom is pointing directly toward $Fe^+$, forming an Si–H–$Fe^+$ angle of 180°. $^4$**4′** differs from $^4$**4** only in the type of bonding of the silane molecule, which in $^4$**4′** is bound by electrostatic interaction between the silicon atom and iron with the Fe–Si bond bisecting the H–Si–H angle. The sextet analog $^6$**4** ($E_{rel}$ = 25.4 kcal $mol^{-1}$) shows a comparable bonding to $SiH_4$, but a different type of bonding to $C_2H_4$, compared to the quartet analogs. The ethylene ligand is not symmetrically bound, but rather an electrostatic interaction exists between C(1) and $Fe^+$, whereas C(2) is directed away from the metal. The silane ligand is also bound through electrostatic interaction, in the same manner as described for $^4$**4**. Generally, the metal–ligand bond lengths in the sextet structures are elongated compared to the quartet structures, which is easily explained by the different bonding situation evoked by the electronic structure of $Fe^+(^6D)$ with its $3d^64s^1$ configuration.

From **4**, the reaction continues either to exit channel **5** + $SiH_4$, which is located at $E_{rel}$ = 9.5 kcal $mol^{-1}$ and $E_{rel}$ = 37.3 kcal $mol^{-1}$ on the quartet and sextet PES, respectively, or to exit channel **6** + $C_2H_4$, located at $E_{rel}$ = 31.5 and 38.1 kcal $mol^{-1}$ on the respective quartet and sextet surfaces. In $^4$**5**, the ethylene ligand shows a typical C–C bond length ($r_{CC}$ = 1.41 Å), and Fe is symmetrically attached to the double bond with $r_{CoC(1)C(2)}$ = 2.09 Å. The structure obtained for $^4$**5** agrees well with the geometrical features of this complex published in earlier calculations [52]; however, the calculated bond-dissociation

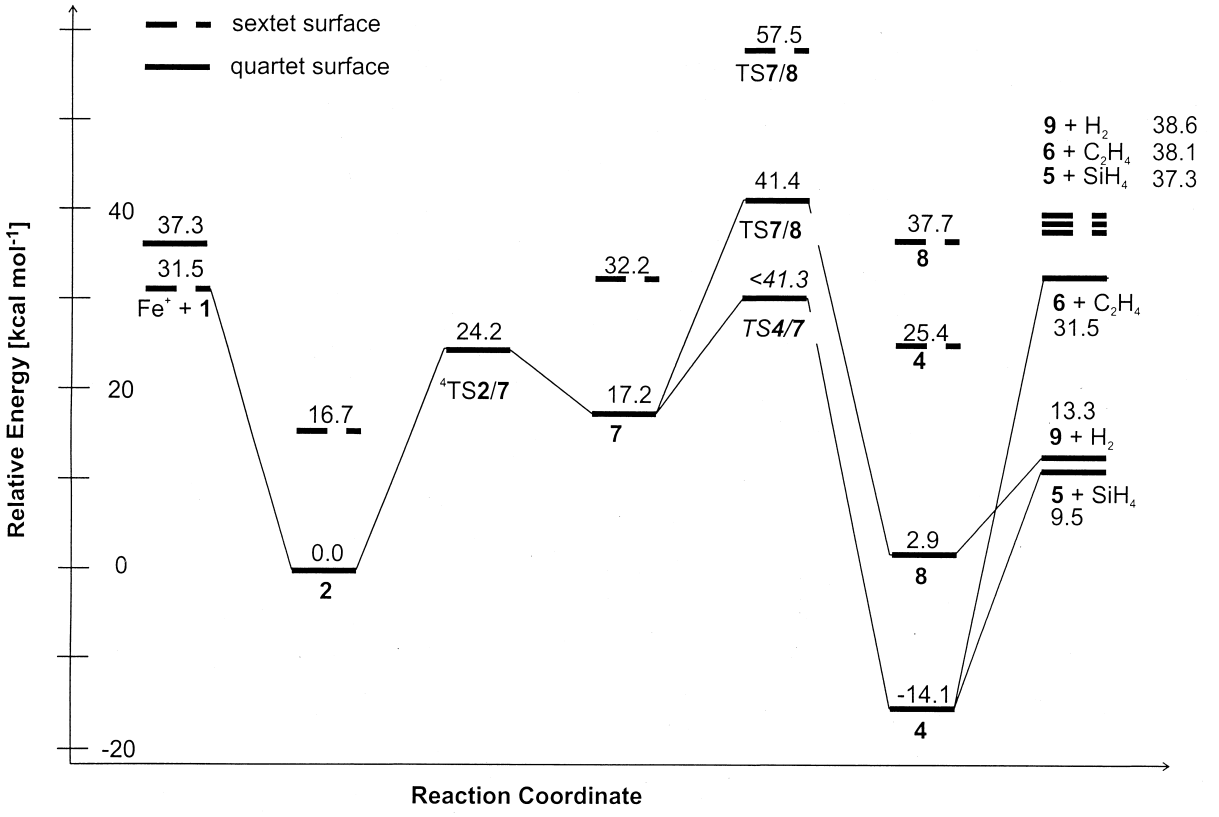


Fig. 4. B3LYP/Ahlrichs PES of the C(2)–H bond insertion pathway of $Fe^+ + C_2H_5SiH_3$ relative to the lowest-lying encounter complex $^4$**2**; see also footnote of Fig. 3.

energy of $D_0 = 51.2$ kcal mol$^{-1}$ deviates strongly from experimental data ($D_0 = 34.6 \pm 2.5$) [53]. The reason for this strong divergence between theory and experiment is most likely that B3LYP fails to adequately describe the $\pi$-bonding interaction between the metal center and the ligand (see above). The sextet exit channel $^6$**5** + $SiH_4$ is not extensively discussed here because it is energetically located well above its corresponding quartet state.

In complex $^4$**6**, $FeSiH_4^+$, the silane ligand is bound through electrostatic $Fe^+$–Si interaction ($r_{FeSi} = 2.41$ Å), with the silicon–iron bond bisecting the H–Si–H angle. The bond energy $D_0(FeSiH_4^+)$ is calculated to 22.4 kcal mol$^{-1}$, which seems reasonable for the expected electrostatic interaction, although no experimental values are available for comparison. The lower stability of $^4$**6** compared to $^4$**5** accounts for the thermodynamic preference of the exit channel $^4$**5** + $SiH_4$ of 22.0 kcal mol$^{-1}$. This theoretical result is supported by the experimental finding that no loss of $C_2H_4$ is observed in either mass spectrometric approach. In contrast to its quartet analog, the sextet species $^6$**6** is bound through a single hydrogen-iron electrostatic interaction, causing a linear Si–H–Fe unit.

### *4.4. C(2)–H bond insertion (Fig. 4)*

On this PES, the reaction commences from **2** toward the inserted structure **7**. $^4$TS**2**/**7** ($E_{rel} = 24.2$ kcal mol$^{-1}$) is a late TS, its structure already resembling the geometry of $^4$**7**. The imaginary frequency of i680 cm$^{-1}$ is mainly accounted for by the shift of the hydrogen atom from C(2) toward $Fe^+$, whereas the

rotational motion of the two hydrogen atoms remaining at C(2) contributes less. Although the sextet $^6$TS**2**/**7** could not be located, a single point calculation of the optimized quartet structure shows a distinctly higher energy for the high-spin state, such that it is assumed not to influence the lowest-energy path of the reaction, and a further search for $^6$TS**2**/**7** is deemed unnecessary.

The major geometry difference of the quartet C(2)–H inserted structure $^4$**7** ($E_{rel}$ = 17.2 kcal mol$^{-1}$) to $^4$TS**2**/**7** is the distinctly widened C–Fe–H angle (see Schemes 1 and 2). In contrast to its quartet analog, the sextet C(2)–H inserted structure $^6$**7** ($E_{rel}$ = 32.2 kcal mol$^{-1}$) adopts an almost linear C–Fe–H unit, thus clearly differing from the corresponding quartet minimum.

From **7**, the reaction may proceed by (1) $\beta$-$SiH_3$ migration via TS**4**/**7** to form complex **4** or by (2) $\beta$-H migration via TS**7**/**8** to form the bisligated complex $Fe^+(H_2)(C_2H_3SiH_3)$ (**8**). Along the first pathway, localization of TS**4**/**7** proved to be very difficult along both PESs. Despite many different input structures and the attempts to localize a sufficiently well-guessed input structure using linear synchronous transit (LST) and quadratic synchronous transit (QST) procedures, no transition structure is found. However, a single-point calculation on the optimized cobalt analog yields an upper limit of $E_{rel} < 41.3$ kcal mol$^{-1}$ for $^4$TS**4**/**7**. Because the single-point calculation for the corresponding sextet TS is even higher in energy, it seems reasonable to neglect involvement of the sextet surface. The upper limit obtained from the cobalt analog is well able to explain the experimentally observed features, and, although it is not satisfying to resign without locating this structure, the given upper limit for $^4$TS**4**/**7** is used due to limited computer resources. After passing TS**4**/**7**, the reaction continues toward minimum **4** and further to the products **5** and **6** (see above).

The second feasible pathway, i.e. the $\beta$-H migration starting from **7** passes via TS**7**/**8** toward minimum **8**. On the quartet surface, $^4$TS**7**/**8** ($E_{rel}$ = 41.4 kcal mol$^{-1}$) shows a distinctly elongated bond of $r_{C(1)H}$ = 1.35 Å pointing toward the Fe–H unit. Frequency analysis shows that the imaginary mode (i1053 cm$^{-1}$) corresponds mainly to the movement of the two hydrogen atoms approaching each other. Smaller contributions to the transition mode result from the shortening of the C–C bond. In analogy, one C–H bond at C(1) is distinctly elongated ($r_{C(1)H}$ = 1.35 Å) in $^6$TS**7**/**8** ($E_{rel}$ = 57.5 kcal mol$^{-1}$) and the H–H distance amounts to only 1.09 Å, indicating that the sextet TS is even later on the reaction coordinate than in its quartet analog ($r_{HH}$ = 1.45 Å). The strong imaginary frequency for $^6$TS**7**/**8** of i1332 cm$^{-1}$ can be attributed—in analogy to the quartet counterpart—to the approach of the two hydrogen atoms at $Fe^+$ with smaller contributions due to rotational rearrangement of the hydrogen atoms at C(1). Following TS**7**/**8**, complex **8** is reached, which consists of an iron cation surrounded by an $H_2$ ligand and a $C_2H_3SiH_3$ moiety. The corresponding quartet and sextet species are located 2.9 kcal mol$^{-1}$ and 37.7 kcal mol$^{-1}$. In $^4$**8**, the $\pi$-type bonding of the $C_2H_3SiH_3$ subunit to iron is demonstrated by almost symmetrical Fe–C bonds, $r_{FeC(1)}$ = 2.09 Å and $r_{FeC(2)}$ = 2.12 Å, in analogy to the iron-ethylene complex $^4$**5**. The slight distortion of the iron-ethylene unit from ideal symmetry can be attributed to the influence of the $SiH_3$ group on C(1). In contrast, in $^6$**8** the $C_2H_3SiH_3$ unit is bound strongly asymmetric with $r_{FeC(1)}$ = 3.08 Å and $r_{FeC(2)}$ = 2.34 Å, such that the structure can be interpreted as a $\sigma$-type bonding between $Fe^+$ and C(2), an assignment that is also supported by the NBO (natural bond orbital) analysis. Again, the tendency for $Fe^+(^6D)$ to arrange the fragments in a linear manner is noticeable.

Dissociation of $^4$**8** results in loss of $H_2$ and formation of the product **9**. The exit channel is located at $E_{rel}$ = 13.3 kcal mol$^{-1}$ and 38.6 kcal mol$^{-1}$ on the respective quartet and sextet PES. In $^4$**9**, the slightly asymmetric bonding in analogy to $^4$**8** is again manifested ($r_{FeC(1)}$ = 2.03 Å and $r_{FeC(2)}$ = 2.11 Å), but $r_{CC}$ = 1.42 Å still points to a carbon–carbon double bond. In contrast, the $C_2H_3SiH_3$ unit of complex $^6$**9** is asymmetrically bound to iron, as is already observed in $^6$**8**. However, in contrast to $^6$**8**, in $^6$**9** the bond lengths are reversed, i.e. $r_{FeC(1)}$ = 2.37 Å and $r_{FeC(2)}$ = 2.95 Å. Although this effect is very interesting, because the $H_2$ ligand on iron seems to reverse the location of the electrophilic attack onto the double

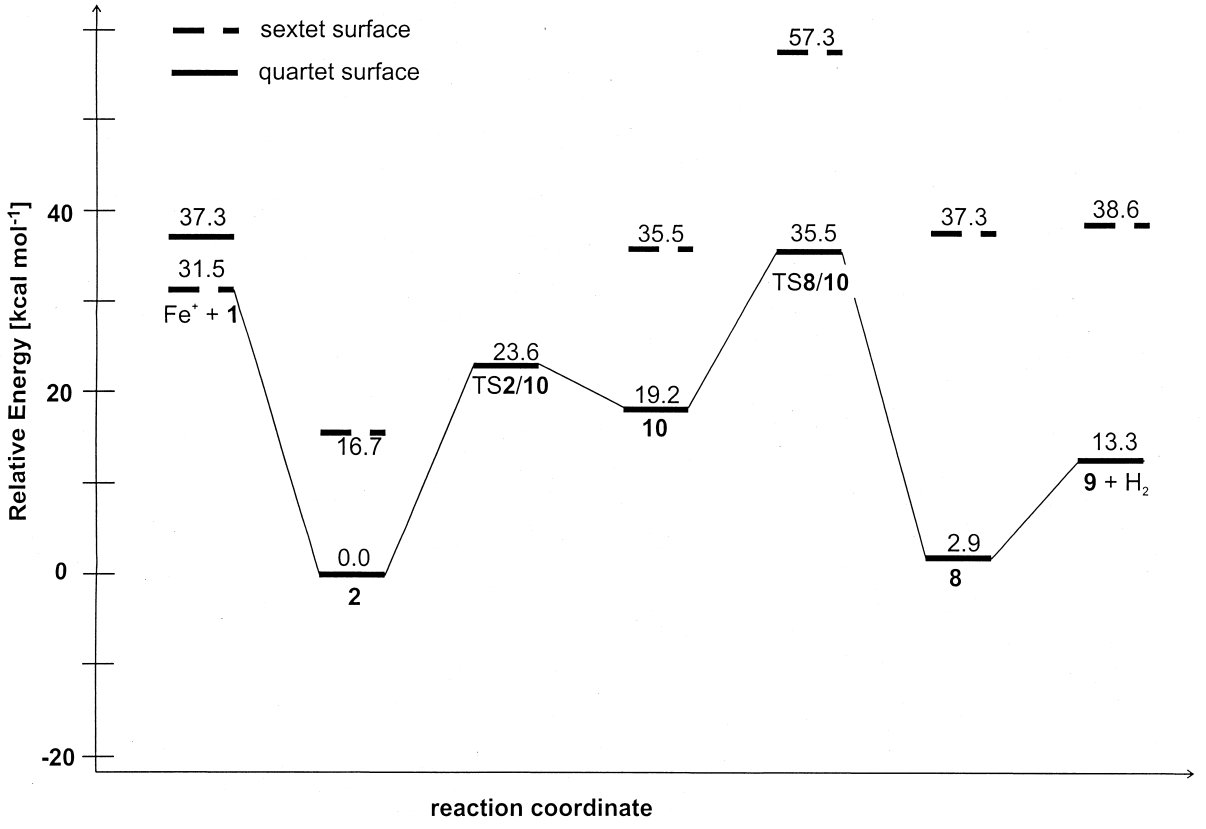


Fig. 5. B3LYP/Ahlrichs PES of the C(1)–H bond insertion pathway of $Fe^+ + C_2H_5SiH_3$ relative to the lowest-lying encounter complex $^4$**2**; see also footnote of Fig. 3.

bond, the ground state of this product channel is clearly the quartet analog, $^4$**9** + $H_2$, such that a detailed investigation of the sextet system is not further pursued.

### *4.5. C(1)–H bond insertion (Fig. 5)*

This pathway involves the following minima and transition structures (in the order of their appearance): TS**2**/**10**, **10**, TS**8**/**10**, **8**, and **9**. In $^4$TS**2**/**10** ($E_{rel}$ = 23.6 kcal mol$^{-1}$), the metal atom approaches the C–H bond to be activated, which is already almost broken ($r_{CH}$ = 1.77 Å), see Scheme 2. The imaginary frequency of the TS (i611 cm$^{-1}$) corresponds to widening the C(1)–Fe–H angle; in addition, the rotational rearrangement of the atoms connected to C(1) contributes to the imaginary mode to some extent. Whereas the sextet analog of $^4$TS**2**/**10** could not be located despite many attempts, a single-point calculation onto the optimized quartet structure exhibited a much higher energy than $^4$TS**2**/**10**, such that the assumption of a quartet ground state for TS**2**/**10** seems justified.

Minimum **10** is located at $E_{rel}$ = 19.2 kcal mol$^{-1}$ and $E_{rel}$ = 35.5 kcal mol$^{-1}$ on the quartet and sextet surfaces, respectively. Although the structure of $^4$**10** resembles very much the corresponding $^4$TS**2**/**10**, $^6$**10** exhibits an almost linear C–Fe–H unit. The subsequent transition structure TS**8**/**10** again shows a distinctly lower energy for the quartet than for the sextet state ($E_{rel}$ = 35.5 versus 57.3 kcal mol$^{-1}$). $^4$TS**8**/**10** shows a very elongated C(2)–H bond with the hydrogen atom pointing toward the metal-hydrogen unit. The H–H distance is 1.48 Å, much longer than a normal H–H bond, thus the TS appears early on the reaction coordinate. The imaginary frequency (i1084 cm$^{-1}$) is assigned to the motion of the two hydrogen

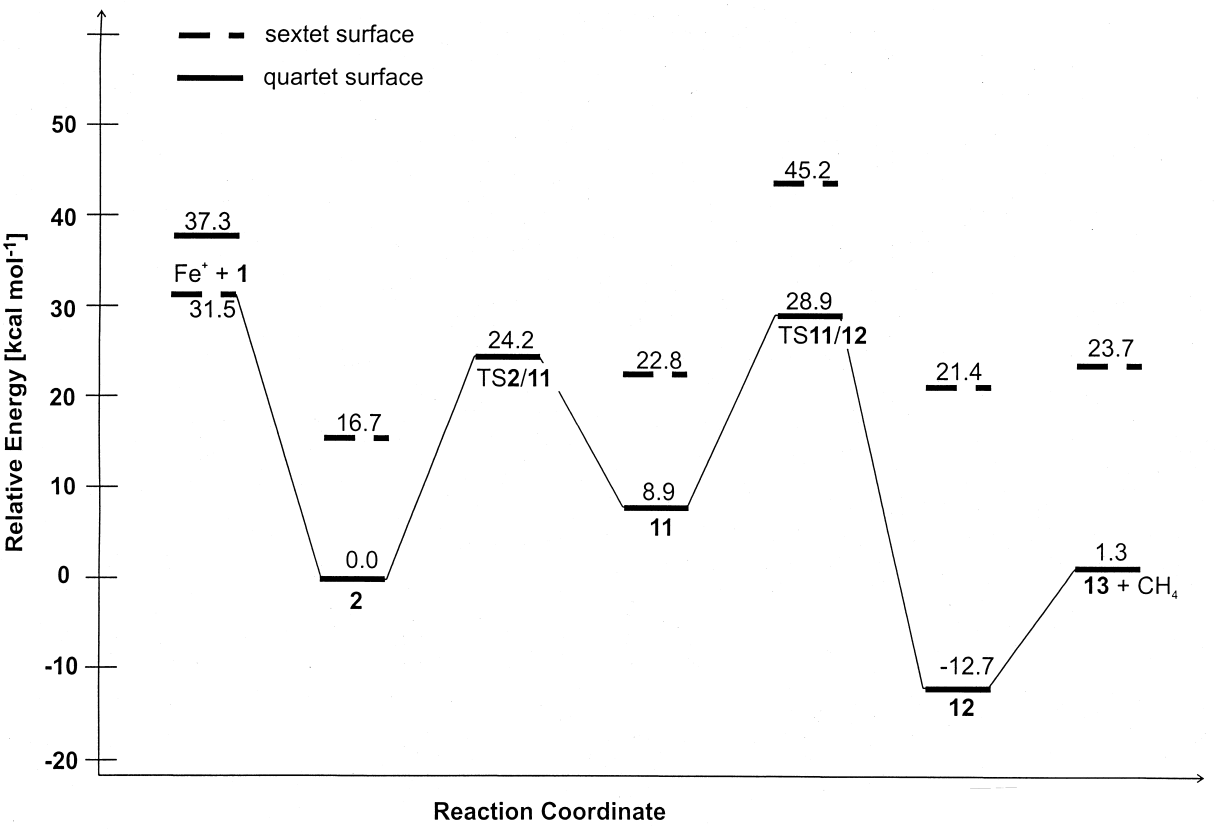


Fig. 6. B3LYP/Ahlrichs PES of the C–C bond insertion pathways of $Fe^+ + C_2H_5SiH_3$ relative to the lowest-lying encounter complex $^4$**2**; see also footnote of Fig. 3.

atoms approaching each other with smaller contributions from the rotational rearrangement of the hydrogen atoms at C(2). In contrast to its quartet analog, $^6$TS**8**/**10** is a late TS on the reaction coordinate as demonstrated by the small H–H distance of only 1.12 Å. In analogy to the quartet structure, one C(2)–H bond points toward the metal and is significantly elongated. The motion of the two hydrogen atoms approaching each other accounts for the imaginary frequency of i1418 $cm^{-1}$. Complex **8** may easily decompose by losing molecular hydrogen and forming product **9**. These structures have been described above and are therefore not repeated.

### *4.6. C–C bond insertion (Fig. 6)*

The reaction on the quartet surface first traverses TS**2**/**11** to yield the C–C inserted structure **11**. In the quartet $^4$TS**2**/**11** ($E_{rel}$ = 24.2 kcal $mol^{-1}$), the metal ion approaches the C–C bond, and in the course of this motion the C–C bond is weakened and thus strongly elongated (from $r_{CC}$ = 1.54 Å in $^4$**2** to $r_{CC}$ = 2.01 Å in $^4$TS**2**/**11**). The imaginary frequency (i385 $cm^{-1}$) is attributed to the motion of the two C(1) and C(2) moieties away from each other. The sextet analog of this TS could not be localized despite many attempts; however, comparison with the other insertion pathways as well as with earlier work on the activation of ethane and propane by "bare" iron atoms [38–40] allows the assumption that the quartet TS is likely to be lower in energy than the corresponding sextet. Thus, further investigation of the sextet TS is not pursued.

The reaction then proceeds toward the C–C inserted minimum **11**. The quartet isomer $^4$**11** ($E_{rel}$ =

8.9 kcal mol$^{-1}$) shows *anti*-conformation with respect to the Fe–C(1) bond. The two metal-carbon bonds are almost symmetric ($r_{FeC(1)}$ = 1.93 Å and $r_{FeC(2)}$ = 1.97 Å); the shorter Fe–C(1) bond is attributed to the electron withdrawing properties of the silyl moiety, weakening the Fe–C(1) bond. The sextet isomer, $^{6}$**11** ($E_{rel}$ = 22.8 kcal mol$^{-1}$), shows a linear C(1)–Fe–C(2) unit ($\alpha_{C(1)FeC(2)}$ = 179°) with both Fe–C and Fe–H bonds elongated as compared to the corresponding quartet structure. Next along the reaction path is TS**11**/**12**, whose respective quartet and sextet isomers are located at $E_{rel}$ = 28.9 and 45.2 kcal mol$^{-1}$. $^{4}$TS**11**/**12** shows one dramatically elongated Si–H bond in conjunction with a preformed iron-hydrogen bond. This suggests that the actual hydrogen migration occurs in two steps, the first one being the migration from the silyl-group to iron and the second step consisting of the hydrogen shift from iron to the methyl-moiety. However, the structure showing an iron-hydrogen bond is not a true minimum but a TS that is supported by the IRC calculations connecting $^{4}$TS**11**/**12** with $^{4}$**12**. $^{6}$TS**11**/**12** is a very early TS, in which the Si–H bond is only slightly elongated and iron-hydrogen distance is quite large. Here again, IRC calculations prove the assignment of this TS to the migration of the hydrogen atom from the silyl to the methyl group. The rather small imaginary mode of i317 cm$^{-1}$ corresponds to the motion of the hydrogen atom away from $SiH_3$ toward the methyl in combination with a rotation of the $CH_3$ group.

The reaction further continues to minimum **12**, whose quartet and sextet isomers are located at $E_{rel}$ = −12.7 kcal mol$^{-1}$ and 21.4 kcal mol$^{-1}$, respectively. These complexes consist of the metal ion surrounded by a methane and a silaethylene ligand. The methane is bound through electrostatic Fe$^{+}$–C interactions. In $^{4}$**12**, the short Si–C bond of 1.81 Å in the silaethylene ligand points to the nominal formation of a C–Si double bond [54,55], which can then bind through $\pi$ interaction to the metal center. Quasisymmetric $\pi$ interaction is supported by the Fe–C and Fe–Si bond lengths ($r_{FeC}$ = 2.01 Å and $r_{FeSi}$ = 2.67 Å), where the longer Fe–Si bond accounts for the larger volume of the silicon compared to carbon. In contrast, the silaethylene ligand does not form a $\pi$ bond to the metal in minimum $^{6}$**12**. Instead, electrostatic interaction occurs between Fe$^{+}$ and C(1) ($r_{FeC(1)}$ = 2.00 Å), while the $SiH_3$ group is pointing away from the metal ($r_{FeSi}$ = 3.42 Å). From minimum **12**, the exit channel **13** + $CH_4$ ($E_{rel}$ = 1.3 kcal mol$^{-1}$ and 23.7 kcal mol$^{-1}$ for the quartet and sextet states, respectively) is easily reached by simple dissociation. The structure of $^{4}$**13** is very close to that of $^{4}$**12**. This is easily explained because no significant change in the electronic structure is expected from loss of the only weakly electrostatically bound methane molecule.

## 5. Discussion

Let us first outline the general features of the investigated PESs. (1) As evidenced from the energetic demand of the calculated sextet species, the sextet PES does not play a role for the ground-state reactivity of the system along all four primary insertion pathways. This is in good agreement with earlier reports by Holthausen et al. [38–40], who found the low-spin PES to dominate the activation of ethane and propane by "bare" Fe$^{+}$. Although not all of the conceivable sextet transition structures have been located in this study, there is no reason to doubt this conjecture. Therefore, although the iron cation in the entrance channel does exhibit a sextet ground state, a spin crossing to the quartet PES occurs between the entrance channel and the encounter complex and from there on the whole reaction continues along the low-spin PES. (2) In analogy to the Co$^{+}$/ethylsilane system, the quartet minima are located well below the entrance channel. Thermochemically, formation of $^{4}$**13** + $CH_4$ is the lowest-lying exit channel at 1.3 kcal mol$^{-1}$, which is for the most part due to the stability of the neutral, but also because of the $\pi$-type interaction in $Fe(CH_2SiH_2)^{+}$ with $D_0(Fe^{+}\text{-}CH_2SiH_2)$ = 30.2 kcal mol$^{-1}$. (3) On the quartet C–C bond insertion pathway, all transition structures are calculated to lie below the entrance channel; the reaction exothermicity for formation of $^{4}$**13** + $CH_4$ is calculated to be 2.6 kcal mol$^{-1}$. (4) The pathways of primary C–Si and C(1)–H bond insertions are calculated to occur at only slightly elevated energies that

may already be reached under thermal conditions. For the C(2)–H bond insertion pathway, however, calculated barriers of 9.9 and <9.8 kcal $mol^{-1}$ in excess of the entrance-channel energy render the progression of the reaction along this pathway unlikely. (5) In agreement with other calculations on the activation of nonpolar organic substrates, the initial step of insertion into a bond of the substrate is not rate determining. With regard to these general aspects, the following discussion concentrates on the quartet surface, with the most attention paid to the rate determining transition structures and the exit channels. The discussion follows the experimentally observed formation of individual products.

### 5.1. Demethanation

For the loss of $CH_4$, only the pathway of initial C–C bond insertion and subsequent $\beta$-hydrogen migration is calculated. The reverse pathway, i.e. primary Si–H bond insertion and subsequent methyl-migration, is not considered for two reasons. (1) Initial Si–H bond insertion would require formation of a stable species where $Fe^+$ is inserted into a Si–H bond. As concluded above, however, such a reaction is likely to continue directly toward insertion into another Si–H bond and formation of the silylidene, $^4$**14**. (2) Generally, it has been shown in earlier work, that migration of an alkyl group is energetically more demanding than migration of a hydrogen atom [40,56,57].

The exit channel of the C–C insertion process is located 30.2 kcal $mol^{-1}$ below the entrance channel, such that the location of the transition structures determines the reactivity of the system along this pathway. The critical TS along the C–C bond insertion surface is $^4$TS**11**/**12**, which is located 2.6 kcal $mol^{-1}$ below the entrance channel, thus being consistent with a slightly exothermic reaction, in good agreement with the experimental results.

### 5.2. Dehydrogenation

For loss of $H_2$, three different reaction pathways are conceivable of which the Si–H insertion pathway concomitant with formation of a silylidene complex is excluded on experimental grounds. The remaining pathways, i.e. initial C(1)–H and C(2)–H bond insertions, lead to $Fe(C_2H_3SiH_3)^+$ ($^4$**9**) as the ionic product complex. The critical TSs along the C(1)–H and C(2)–H insertion pathways are $^4$TS**8**/**10** and $^4$TS**7**/**8** at 35.5 and 41.4 kcal $mol^{-1}$, respectively. These energies are 0 K values, and it is obvious that at thermal energies $^4$TS**8**/**10** may be overcome, although $^4$TS**7**/**8** is too high in energy to allow this pathway to participate in the formation of $H_2$. Therefore, it is concluded that dehydrogenation occurs mainly via the C(1)–H bond insertion pathway and that the barrier height accounts for the experimentally observed weakness of $H_2$ loss.

### 5.3. Loss of $SiH_4$

Two of the reaction pathways calculated lead to formation of the ionic product species $Fe(C_2H_4)^+$ concomitant with loss of neutral $SiH_4$, i.e. primary Si–H and C(2)–H bond insertions. In both pathways, $Fe(C_2H_4)(SiH_4)^+$ is the key intermediate that has, in fact, two obvious possibilities to dissociate by loss of silane or ethylene, respectively. However, the hypothetical formation of $Fe(SiH_4)^+$ is thermochemically handicapped due to the superior stability of the $Fe(C_2H_4)^+$ complex. Whereas small amounts of $Fe(C_2H_4)^+$ are indeed observed in both sector-MS and FTICR experiments, no indication for formation of $Fe(SiH_4)^+$ is found, even in collisional activation experiments. The critical TSs toward formation of $Fe(C_2H_4)(SiH_4)^+$ are $^4$TS**3**/**4** and $^4$TS**4**/**7** along the C–Si and C(2)–H bond-insertion pathways, respectively. The former is located 3.4 kcal $mol^{-1}$ above the ground-state entrance channel, although for the latter, a limit of only <41.3 kcal $mol^{-1}$ is known. Because $^4$TS**3**/**4** is located slightly above the entrance channel, this is a 0 K energy and it is thus quite plausible that the reaction may occur at room temperature, although with a presumably low reaction rate. This is in good agreement with the experimental data that show only very minor intensities of the $Fe(C_2H_4)^+$ fragment (1–4%). As for the second conceivable pathway, only an energy limit for $^4$TS**4**/**7** is known and it cannot be determined unambiguously whether or not the C(2)–H

bond insertion pathway contributes to the observed $Fe(C_2H_4)^+$ fragment. However, a comparison to the related $Co^+$/ethylsilane system indicates that the TS for the C(2)–H bond insertion pathway is distinctly higher in energy than the TS of the C–Si bond insertion pathway, and thus does not contribute to the silane loss [25]. Although comparison between both metals is somewhat difficult, as is demonstrated by the different experimental results, the hitherto calculated reaction pathways show very similar features for iron and cobalt. It is therefore reasonable to assume that this similarity can be transferred to the C–Si bond insertion pathway, i.e. $Fe(C_2H_4)^+$ is preferentially formed via the C–Si bond insertion pathway.

### *5.4. Comparison of the product channels*

For all four pathways, the migration TSs are much higher in energy than the respective product channels. In addition, the TSs of the C–Si, C(1)–H, and C–C bond-insertion pathways are located in the same energy range, given the error of the calculations of $\pm 6$ kcal $mol^{-1}$. Thus, strong competition can be expected between these routes. Although quantitative assessment of the branching ratios is difficult, demethanation is suggested as the dominating channel. In contrast, dehydrogenation and loss of silane are predicted as minor products. The calculations find the corresponding TSs $^4$TS**8**/**10** and $^4$TS**3**/**4** at a very small energy splitting of only 0.6 kcal $mol^{-1}$ with a preference for $^4$TS**3**/**4** of the silane loss. This energy splitting is clearly within the error of the calculations and several reasons are conceivable for the contradictory preponderance of $H_2$ loss in the experiments: (1) within the error of the calculations $^4$TS**8**/**10** may be calculated too high in energy and $^4$TS**3**/**4** too low, or (2) because all energies are given at 0 K, entropy effects may reverse the sequence of the two TSs when including the experimental temperatures of 298 K.

## 6. Conclusions

The reaction of $Fe^+$ with ethylsilane is investigated at the B3LYP/Ahlrichs level of theory. Qualitative and semiquantitative agreement is reached between the experiments and the calculations in that all experimentally observed products are calculated to be formed along exothermic or slightly endothermic pathways at 0 K, the latter being so close in energy to the entrance channel that the associated barriers are surmountable at room temperature (298 K). Moreover, loss of $CH_4$ after primary C–C bond insertion is the dominating product, both experimentally and in the calculations. The favored pathways of the losses of $H_2$ and $SiH_4$ are the C(1)–H and Si–H bond insertions, respectively. Primary C(2)–H insertion is ruled out for the dehydrogenation product but may occur to some extent en route to the formation of $Fe(C_2H_4)^+$. Both the C(1)–H and Si–H bond insertion pathways are associated with comparable energy demands such that unambiguous assignment of the computationally preferred product is not possible within the accuracy of the calculations.

In addition, the present work allows some more general evaluation of the performance of DFT calculations as a tool to interpret and/or predict the reactivity of transition-metal containing systems. As shown from the above $Fe^+$/ethylsilane example, B3LYP does indeed allow one to describe these systems as qualitatively correct. In fact, although dissimilar channels may exhibit different systematic errors, these seem to cancel each other out to a large extent in the present system. In comparison to our earlier work on $Co^+$/ethylsilane, however, where only a qualitative agreement between theory and experiment was reached, it remains to note that despite all progress in recent years, the quantitative description of competing processes with DFT is, in many cases, still problematic. Nevertheless, at present, even high-level *ab initio* theoretical approaches cannot guarantee a less erratic quantitative description of branching ratios; consequently DFT appears as a good compromise between the desired accuracy of the calculations and the existing computational resources.

## Acknowledgements

Financial support by the Deutsche Forschungsgemeinschaft, the Fonds der Chemischen Industrie and the Volkswagen-Stiftung is gratefully acknowledged.

We thank Dr. Ilona Kretzschmar for helpful discussions. Generous allocation of computer time by the Konrad-Zuse Zentrum Berlin is appreciated.

## References

[1] A.E. Shilov, Activation of Saturated Hydrocarbons by Transition Metal Complexes, Reidel, Boston, MA, 1984.
[2] C.L. Hill, Activation and Functionalization of Alkanes, Wiley, New York, 1989.
[3] J.A. Davies, P.L. Watson, J.F. Liebmann, A. Greenberg (Eds.), Selective Hydrocarbon Activation, VCH, Weinheim, 1990.
[4] D.H.R. Barton, Aldrichimica Acta 23 (1990) 3.
[5] R.H. Crabtree, Chem. Rev. 85 (1985) 245.
[6] F. Garin, G. Maire, Acc. Chem. Res. 22 (1989) 100.
[7] B.A. Arndtsen, R.G. Bergmann, T.A. Mobley, T.H. Peterson, Acc. Chem. Res. 28 (1995) 154.
[8] A.E. Shilov, G.B. Shulpin, Chem. Rev. 97 (1997) 2879.
[9] B. Rybtchinski, D. Milstein, Angew. Chem. 38 (1999) 870.
[10] H. Chen, S. Schlecht, T.C. Semple, J.F. Hartwig, Science 287 (2000) 1992.
[11] H.M.L. Davies, T. Hansen, M.R. Churchill, J. Am. Chem. Soc. 122 (2000) 3063.
[12] K. Eller, H. Schwarz, Chem. Rev. 91 (1991) 1121.
[13] K. Eller, Coord. Chem. Rev. 126 (1993) 93.
[14] B.S. Freiser, Acc. Chem. Res. 27 (1994) 353.
[15] K. Morokuma, K. Ohta, N. Koga, S. Obara, E.R. Davidson, Faraday Symp. Chem. Soc. 19 (1984) 84.
[16] E. Folga, T. Ziegler, Can. J. Chem. 70 (1992) 333.
[17] P.E.M. Siegbahn, M.R.A. Blomberg, M. Svensson, J. Am. Chem. Soc. 115 (1993) 1952.
[18] J.J. Carroll, K.L. Haug, J.C. Weisshaar, M.R.A. Blomberg, P.E.M. Siegbahn, M.J. Svensson, J. Phys. Chem. 99 (1995) 13 955.
[19] M.C. Holthausen, W. Koch, J. Am. Chem. Soc. 118 (1996) 9932.
[20] M. Brönstrup, D. Schröder, H. Schwarz, Chem. Eur. J. 6 (2000) 91.
[21] M. Brönstrup, C. Trage, D. Schröder, H. Schwarz, J. Am. Chem. Soc. 122 (2000) 699.
[22] G. Hornung, D. Schröder, H. Schwarz, J. Am. Chem. Soc. 119 (1997) 2273.
[23] R.H. Hertwig, K. Seemeyer, H. Schwarz, W. Koch, Chem. Eur. J. 3 (1997) 1315.
[24] G. Hornung, S. Bärsch, D. Schröder, H. Schwarz, Organometallics 17 (1998) 2271.
[25] S. Bärsch, T. Böhme, D. Schröder, H. Schwarz, Int. J. Mass. Spectrom., 199 (2000) 107.
[26] M.J. Frisch, G.W. Trucks, H.B. Schlegel, P.M.W. Gill, B.G. Johnson, M.A. Robb, J.R. Cheeseman, T.A. Keith, G.A. Petersson, J.A. Montgomery, K. Raghavachari, M.A. Al-Laham, V.G. Zakrzewski, J.V. Ortiz, J.B. Foresman, J. Cioslowski, B.B. Stefanov, A. Nanayakkara, M. Challacombe, C.Y. Peng, P.Y. Ayala, W. Chen, M.W. Wong, J.L. Andres, E.S. Replogle, R. Gomperts, R.L. Martin, D.J. Fox, J.S. Binkley, D.J. Defrees, J. Baker, J.P. Stewart, M. Head-Gordon, C. Gonzalez, J.A. Pople, GAUSSIAN 94, Revision A.1, Gaussian Inc., Pittsburgh, PA, 1995.
[27] C. Lee, W. Yang, R.G. Parr, Phys. Rev. B 37 (1988) 785.
[28] B. Miehlich, A. Savin, H. Stoll, H. Preuss, Chem. Phys. Lett. 157 (1989) 200.
[29] A.D. Becke, J. Chem. Phys. 98 (1993) 5648.
[30] M.C. Holthausen, G. Hornung, D. Schröder, S. Sen, W. Koch, H. Schwarz, Organometallics 16 (1997) 3135.
[31] W. Koch, M.C. Holthausen, A Chemists Guide to Density Functional Theory, Wiley-VCH, Weinheim, 2000.
[32] A. Schafer, H. Horn, R. Ahlrichs, J. Chem. Phys. 97 (1992) 2571.
[33] "Standard" refers to the default setting in GAUSSIAN 94: Max. force = 0.00045; RMS force = 0.00030; Max. displacement = 0.00180; RMS displacement = 0.00120.
[34] K. Fukui, J. Phys. Chem. 74 (1970) 4161.
[35] C. Gonzales, H.B. Schlegel, J. Chem. Phys. 90 (1989) 2154.
[36] S. Bärsch, I. Kretzschmar, D. Schröder, H. Schwarz, P.B. Armentrout, J. Phys. Chem. A 103 (1999) 5925.
[37] C.B. Kellogg, K.K. Irikura, J. Phys. Chem. A 103 (1999) 1150.
[38] M.C. Holthausen, A. Fiedler, H. Schwarz, W. Koch, Angew. Chem. 107 (1995) 2430.
[39] M.C. Holthausen, A. Fiedler, H. Schwarz, W. Koch, J. Phys. Chem. 100 (1996) 6236.
[40] M.C. Holthausen, W. Koch, Helv. Chim. Acta 79 (1996) 1939.
[41] C. Heinemann, Ph.D. Thesis, TU Berlin D83, 1995, and references cited therein.
[42] M.C. Holthausen, C. Heinemann, H.H. Cornehl, W. Koch, H. Schwarz, J. Chem. Phys. 102 (1995) 4931.
[43] M.C. Holthausen, M. Mohr, W. Koch, Chem. Phys. Lett. 240 (1995) 245.
[44] S. Bärsch, D. Schröder, H. Schwarz, Helv. Chim. Acta 83 (2000) 827.
[45] O. Gunnarson, R.O. Jones, Phys. Rev. B 31 (1985) 7588.
[46] T.V. Russo, R.L. Martin, P.J. Hay, J. Chem. Phys. 101 (1994) 7729.
[47] C.W. Bauschlicher Jr., Chem. Phys. 211 (1996) 163.
[48] J. Sugar, C. Corliss, J. Phys. Chem. Ref. Data 14 (1985) 2(suppl.).
[49] A. Hässelbarth, T. Prüsse, H. Schwarz, Chem. Ber. 123 (1990) 209.
[50] A. Hässelbarth, T. Prüsse, H. Schwarz, Chem. Ber. 123 (1990) 213.
[51] G. Hornung, D. Schröder, H. Schwarz, J. Am. Chem. Soc. 119 (1997) 2273.
[52] D. Schröder, A. Fiedler, H. Schwarz, Int. J. Mass Spectrom. Ion Processes 134 (1994) 239.
[53] M.R. Sievers, L.M. Jarvis, P.B. Armentrout, J. Am. Chem. Soc. 120 (1998) 1891.
[54] Y. Apeloig, in The Chemistry of Organic Silicon Compounds, S. Patai, Z. Rappoport (Eds.), Wiley, New York, 1989, p. 103.
[55] Y. Apeloig, M. Karni, T. Müller, in Organosilicon Chemistry II. From Molecules to Materials, N. Auner, J. Weiss (Eds.), VCH, Weinheim, 1996, p. 263.
[56] O. Eisenstein, Y. Jean, J. Am. Chem. Soc. 107 (1985) 1177.
[57] M. Brookhardt, M.L.H. Green, L.-T. Wong, Prog. Inorg. Chem. 36 (1988) 1.